THE JOURNAL OF PHYSICAL CHEMISTRY LETTERS
A JOURNAL OF THE AMERICAN CHEMICAL SOCIETY

pubs.acs.org/JPCL

Letter

Adiabatic Trajectory Approximation: A New General Method in the Toolbox of Mixed Quantum/Classical Theory for Collisional Energy Transfer

Bikramaditya Mandal, Carolin Joy, Dulat Bostan, Alexander Eng, and Dmitri Babikov*

Cite This: *J. Phys. Chem. Lett.* 2023, 14, 817–824

Read Online

ACCESS | Metrics & More | Article Recommendations | Supporting Information

ABSTRACT: A new version of the MQCT program is presented, which includes an important addition, adiabatic trajectory approximation (AT-MQCT), in which the equations of motion for the classical and quantum parts of the system are decoupled. This method is much faster, which permits calculations for larger molecular systems and at higher collision energies than was possible before. AT-MQCT is general and can be applied to any molecule + molecule inelastic scattering problem. A benchmark study is presented for H_2O + H_2O rotational energy transfer, an important asymmetric-top rotor + asymmetric-top rotor collision process, a very difficult problem unamenable to the treatment by other codes that exist in the community. Our results indicate that AT-MQCT represents a reliable computational tool for prediction of collisional energy transfer between the individual rotational states of two molecules, and this is valid for all combinations of state symmetries (such as *para* and *ortho* states of each collision partner).

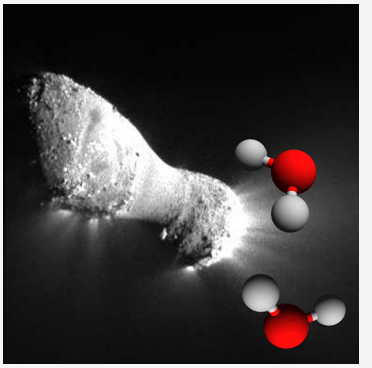

Energy transfer among translational, rotational, and vibrational degrees of freedom during an encounter between two molecules is a fundamentally important process in physical chemistry. Two theoretical methods, known for decades and most frequently used for the description of collisional energy transfer, are the classical trajectory method,[1−4] often called a quasi-classical trajectory, and the full-quantum time-independent inelastic scattering approach,[5−7] called the coupled-channel formalism. Both have their pros and cons. For example, the classical method permits the treatment of large molecular systems[8−12] but has several fundamental flaws such as zero-point energy leakage and violation of microscopic reversibility and lacks many essential features, such as quantization of the internal molecular states, selection rules for state-to-state transitions, quantum interference, and symmetry effects. All of these are present in the full-quantum approach, but the penalty for quantum treatment of scattering is its significant computational cost. In practice, the full-quantum description of collisional energy transfer is feasible only for simple collision partners in the low-energy scattering regime, such as in the coldest parts of interstellar media or in ultracold physics experiments.[13−18] Newer time-dependent quantum methods, such as MCTDH,[19,20] offer a somewhat better scaling (compared to the traditional time-independent coupled-channel formalism) and thus are being actively developed.[21,22] Still, the numerical effort required for the full-quantum treatment of scattering is expected to remain high.

A recently proposed quantum statistical approach[23,24] is one way to avoid the cost of scattering calculations. Another practical alternative, which falls between the standard classical and full-quantum methods, is a recently developed mixed quantum/classical theory (MQCT) approach.[25−31] In this method, the time-dependent Schrödinger equation is used to describe the internal degrees of freedom of molecules (their rotation and vibration), while the mean-field trajectories are used to describe the relative translational motion of two collision partners. In recent years, this approach has been applied to many molecular systems, including diatomic, triatomic, tetra-atomic, and polyatomic molecules colliding with an atom,[23,32−35] and to molecule + molecule collisions, including diatom + diatom[36,37] and asymmetric-top rotor + diatom[24,27,38] collisions, and the most general case of collision between two asymmetric-top rotor molecules.[39,40] It was found, by comparison against the full-quantum calculations, that MQCT is reasonably accurate and much less computationally expensive. It enables calculations for larger molecules and higher collision energies than was possible before. A user-ready general computer code MQCT was released a few years ago.[38]

It is now well established that at high collision energies the results of MQCT are very close to the full-quantum results.[27,31,35,38,41] At lower collision energies, dominated by

Received: November 2, 2022
Accepted: December 8, 2022

https://doi.org/10.1021/acs.jpclett.2c03328
J. Phys. Chem. Lett. 2023, 14, 817–824

Feshbach resonances, MQCT is less accurate but still gives a qualitatively correct description of the collision process.[31] One phenomenon that MQCT cannot describe in principle is quantum tunneling that is important for the formation of "shape" resonances, but this effect is expected to be less relevant for larger and heavier collision partners. In the work done so far, MQCT was applied mostly to the rotational transitions and to the simplest vibrational transitions in diatomic molecules.[42,43] More work is certainly needed to expand MQCT to the vibrational transitions in triatomic molecules and to the coupled rotational−vibrational transition processes.

Importantly, mixed quantum/classical theory represents a general framework that permits the development and testing of new computational methodologies for the description of collisional energy transfer. For example, a very efficient decoupling scheme was recently proposed,[27] which permits to run approximate MQCT calculations for a fraction of the numerical cost of the fully coupled MQCT. This method, named adiabatic trajectory approximation (AT-MQCT), was found to be reliable for H_2O + H_2 rotational energy transfer (including excitation and quenching of both collision partners) and for C_6H_6 + He rotational excitation and quenching in a broad range of rotational excitations and collision energies.[41] One goal of this paper is to expand AT-MQCT to the most general and complex case of asymmetric top + asymmetric top, required for the treatment of molecule + molecule collisions, such as H_2O + H_2O collisions. It should be stressed that no full-quantum scattering results are available for this case, and no quantum codes can handle it, to the best of our knowledge. Therefore, we present a comparison of AT-MQCT versus the fully coupled CC-MQCT method for H_2O + H_2O collisions. Collisional energy transfer in this molecular system is important, in particular, for interpretation of astrophysical observations of molecular species in cometary comae[44] and in atmospheres of icy planets such as Jupiter's moons.[45] Another goal of this paper is to add AT-MQCT to the suite of MQCT_2022 codes (for all 10 system types), to offer a general approach and an efficient computer code for the treatment of rotational transitions in any molecule + molecule system, for potential users in the fields of astrochemistry, atmospheric chemistry, and chemical kinetics in general. Being a time-dependent method, MQCT can provide very useful physical insight into the dynamics of collisional energy transfer in a variety of molecular systems and processes. For this, we present a performance study of AT-MQCT versus CC-MQCT and versus the full-quantum MOLSCAT calculations. Moreover, this paper can also be used as a brief user's guide for the potential users of the MQCT_2022 code. A full version of the user manual is provided in the Supporting Information.

For the sake of completeness, we outline the MQCT equations of motion for classical and quantum degrees of freedom. Rigorous derivation of these formula can be found in the recent literature.[25−35,39,40] A laboratory-fixed reference frame is employed to describe classically the relative motion of two collision partners. Vector $\vec{R}$ connects centers of mass of two collision partners and is described by its length R and azimuthal angle Φ that determines the scattering angle in the equatorial plane (the polar angle is not needed because MQCT trajectories are restricted to one plane due to the cylindrical symmetry of the mean-field potential). R and Φ are classical degrees of freedom, and their evolution is driven by the following classical-like equations of motion (where P_R and P_Φ are generalized momenta associated with R and Φ, respectively):[28,29]

$$\dot{R} = \frac{P_R}{\mu} \tag{1}$$

$$\dot{\Phi} = \frac{P_\Phi}{\mu R^2} \tag{2}$$

$$\dot{P}_R = -\sum_{n'}\sum_{n''} e^{i\varepsilon_{n'}^{n''}t}\sum_m \frac{\partial M_{n'}^{n''}}{\partial R} a_{mn''}^* a_{mn'} + \frac{P_\Phi^{\,2}}{\mu R^3} \tag{3}$$

$$\begin{aligned}\dot{P}_\Phi = -i\sum_{n'}\sum_{n''} e^{i\varepsilon_{n'}^{n''}t}\sum_m M_{n'}^{n''} \\ \times \Big[a_{m-1,n''}^* a_{mn'}\sqrt{j''(j''+1) - m(m-1)} \\ + a_{m+1,n''}^* a_{mn'}\sqrt{j''(j''+1) - m(m+1)} \\ - a_{mn''}^* a_{m-1,n'}\sqrt{j'(j'+1) - m(m-1)} \\ - a_{mn''}^* a_{m+1,n'}\sqrt{j'(j'+1) - m(m+1)}\Big]/2\end{aligned} \tag{4}$$

Multiple sums in eqs 3 and 4 go over all quantum states of the system. $\varepsilon_{n'}^{n''}$ terms correspond to energy differences between the initial (lower index) and final (upper index) internal states of the system, say rotational or ro-vibrational states with energies $E_{n'}$ and $E_{n''}$. Index m labels projections of molecular angular momentum j onto molecule−molecule axis $\vec{R}$ (which is used as quantization axis z in the body-fixed reference frame). Time evolution of quantum states is described in the so-called body-fixed reference frame, the rotating frame tied to molecule−molecule vector $\vec{R}$. Probability amplitudes $a_{mn}(t)$ for molecular quantum states (rotational and ro-vibrational) evolve according to the following quantum-like system of coupled equations:[28,29]

$$\begin{aligned}\dot{a}_{mn''} = -i\sum_{n'} a_{mn'}\mathbf{M}_{n'}^{n''} e^{i\varepsilon_{n''}^{n''}t} \\ - \dot{\Phi}\Big[a_{m-1,n''}\sqrt{j''(j''+1) - m(m-1)} \\ + a_{m+1,n''}\sqrt{j''(j''+1) - m(m+1)}\Big]/2\end{aligned} \tag{5}$$

Summation in the first term of this equation includes quantum state-to-state transitions, within given m, driven by potential coupling matrix $\mathbf{M}_{n'}^{n''}$ that depends parametrically on R (omitted for the sake of clarity). This matrix is real-valued, time-independent, and diagonal in m (also omitted for the sake of clarity):

$$\mathbf{M}_{n'}^{n''}(R) = \langle \Psi_{n''}(\Lambda_1, \Lambda_2)|V(R, \Lambda_1, \Lambda_2)|\Psi_{n'}(\Lambda_1, \Lambda_2)\rangle \tag{6}$$

Wave functions $\Psi_{n'}(\Lambda_1, \Lambda_2)$ and $\Psi_{n''}(\Lambda_1, \Lambda_2)$ correspond to the initial and final states, respectively. They describe rotations of two collision partners relative to the molecule−molecule axis $\vec{R}$ using a set of Euler angles $\Lambda_1 = \{\alpha_1, \beta_1, \gamma_1\}$ and $\Lambda_2 = \{\alpha_2, \beta_2, \gamma_2\}$ for molecules 1 and 2, respectively. Potential energy surface $V(R, \Lambda_1, \Lambda_2)$ is expressed through the same variables. The second term in eq 5 describes transitions between the rotational states with $\Delta m = \pm 1$, driven by classical orbital angular velocity $\dot{\Phi}$, which is the Coriolis coupling effect.

https://doi.org/10.1021/acs.jpclett.2c03328
J. Phys. Chem. Lett. 2023, 14, 817−824

To conduct a meaningful test of the cost of MQCT calculations in comparison with the cost of full-quantum calculations, we picked the $H_2O + H_2$ system, because the full-quantum CC calculations can be carried out for this system type using the standard code MOLSCAT[46,47] and because it was shown that CC-MQCT and AT-MQCT give reliable results for these collision partners.[27] Thus, for the $H_2O + H_2$ system, we carried out MOLSCAT calculations at a total energy of 500 cm^{-1} with a fixed total angular momentum J_{TOT} of 100 but increased the number of rotational states included in the basis. The largest MOLSCAT calculations we finished had 140 states of the $H_2O + H_2$ system with the following maximum values: $j_1 = 13$ (for water) and $j_2 = 4$ (for hydrogen) and $E_{max} = 2000$ cm^{-1} (energy of the upper state in the basis). A set of close to 20 independent runs was performed. The serial version of MOLSCAT was used (very long runs using one processor), and the NERSC Cori Haswell computer system was employed (2.3 GHz Intel Xeon Processor, 128 GB of memory). MQCT calculations were done in parallel using 10 processors of the same computer system at the same collision energy and with the same J_{TOT} (which corresponds to the maximum impact parameter of ~25 Bohr and requires 101 MQCT trajectories). Again, the number of rotational states in the basis set was varied, reaching 200 states as the maximum for CC-MQCT and 300 states as the maximum for AT-MQCT calculations. This was sufficient to see the trends.

It is important to stress that the state-to-state transition matrix $\mathbf{M}^{n''}_{n'}$ in MQCT formalism does not depend on orbital angular momentum l. MQCT trajectories with different values of l are propagated independently and use the same matrix, for any choice of l_{max}. This is different from the full-quantum method, in which the size of the matrix depends on J_{TOT}. The only common physical indicator, present in both MQCT and MOLSCAT calculations, is the number of states in the system. Therefore, the comparison of performance in Figure 1 is presented as a function of the number of rotational states. From Figure 1, we can see that when the number of states exceeds 100, the cost of full-quantum calculations increases as N^6, where N is the number of rotational states. In the range of $N \sim 150$, the cost of full-quantum calculations is 4 orders of magnitude higher than the cost of AT-MQCT. It should also be emphasized that MQCT calculations are intrinsically parallel and can be carried out using ≤1000 processors with minimal communication overhead, which reduced the wall-clock time by an additional 3 orders of magnitude. In contrast, the full-quantum calculations are hard to parallelize. While custom versions of parallel MOLSCAT exist among users, the standard version we used was serial.

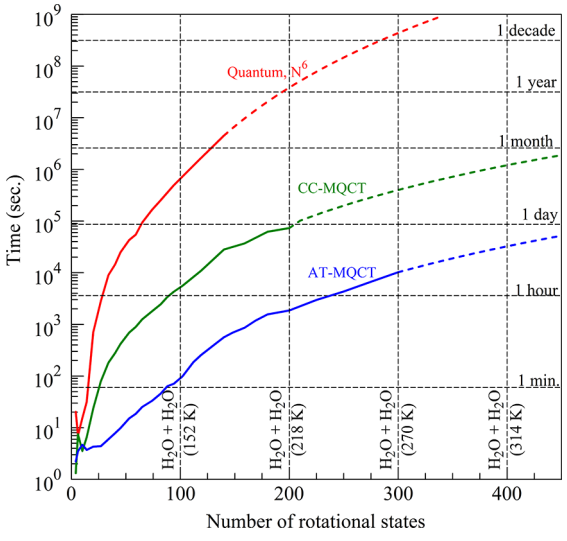

Figure 1. Numerical cost of two versions of MQCT calculations vs full-quantum calculations (MOLSCAT), for molecular systems of increasing complexity (number of rotational states). Calculations are done using the $H_2O + H_2$ system, and a projection for the $H_2O + H_2O$ system is made.

In the range of $N \sim 300$ states, the cost of AT-MQCT increases as N^3, which is a much more favorable scaling law compared to that of the full-quantum calculations (see Figure 1). For example, for the $H_2O + H_2O$ system, we found that AT-MQCT calculations with $N > 1000$ states remain feasible. In Figure 1, we also projected the cost of calculations for the $H_2O + H_2O$ system at various temperatures, assuming that the basis set size should be on the order of $4kT$, or $E_N = 4kT$, where E_N is energy of rotational state number N in the $H_2O + H_2O$ system (see below).

Next, we conducted a test of the accuracy of the approximate AT-MQCT method by comparing its results against the results of the fully coupled CC-MQCT method. For these calculations, we included 12 states of the "target" water molecule up to $j_1 = 3$ (six *para* states and six *ortho* states) combined with 28 states of the "quencher" water molecule up to $j_2 = 6$ (14 *para* states and 14 *ortho* states). Due to symmetry considerations, four independent calculations can be carried out in this case for the *p*-target + *p*-quencher, *p*-target + *o*-quencher, *o*-target + *p*-quencher, and *o*-target + *o*-quencher combinations [84 channels of the $H_2O + H_2O$ system formed in each case (six states of the target combined with 14 states of the quencher)], with a total rotational energy of ≲620 cm^{-1}. This rotational basis set is not that large, considering the well depth of the $H_2O + H_2O$ PES (on the order of 1800 cm^{-1}), but is sufficient to compare two versions of MQCT. Convergence of cross sections with respect to the basis set size is within 40% on average.

For the water + water system, we used the CCpol-8sf[2014] PES from refs 48 and 49. This PES was expanded over the basis set of analytic functions listed in Table 8 of the user manual (see the Supporting Information) for SYS_TYPE = 0 and using the keyword IDENTICAL_PES = YES (see page 21 of the user manual) to take advantage of the PES symmetry imposed by two identical collision partners. We retained 28 symmetrized expansion terms (λ_1, μ_1, λ_2, μ_2, λ) that contain 84 individual functions included in the expression for SYS_TYPE = 0 in Table 8 of the user manual. For example, a symmetrized expansion term with $\mu_1 = 4$ and $\mu_2 = 2$ contains four individual functions expressed through the products of D-functions for collision partners one (1) and two (2): with $\mu(1) = +4$ and $\mu(2) = +2$, with $\mu(1) = -4$ and $\mu(2) = -2$, with $\mu(1) = +4$ and $\mu(2) = -2$, and finally with $\mu(1) = -4$ and $\mu(2) = +2$. This expansion has 23 unique coefficients listed in Table 1 and includes a majority of the dipole and quadrupole interaction terms (λ_1 and λ_2 up to 2) as well as some higher-order interaction terms (λ_1 and λ_2 up to 4). The largest value of the total λ included was 6. The definition of D-functions is given on page 5 of the user manual (see the Supporting Information).

The dependencies of 23 expansion coefficients on the molecule−molecule distance $v_{\lambda_1\mu_1\lambda_2\mu_2\lambda}(R)$ are plotted in Figure

https://doi.org/10.1021/acs.jpclett.2c03328
J. Phys. Chem. Lett. 2023, 14, 817−824

Table 1. Values of the Expansion Coefficients for the PES of the H_2O + H_2O System at R = 8.09 Bohr[a]

	$(\lambda_1, \mu_1, \lambda_2, \mu_2, \lambda)$	$v_{\lambda_1\mu_1\lambda_2\mu_2\lambda}$ (cm^{-1})
$\lambda_1 = 0$	(0, 0, 0, 0, 0)	−4774.19
$\lambda_1 = 1$	(1, 0, 0, 0, 1)	544.31
	(1, 0, 1, 0, 0)	−131.69
	(1, 0, 1, 0, 2)	−14250.92
$\lambda_1 = 2$	(2, 0, 1, 0, 3)	−342.14
	(2, 2, 1, 0, 3)	4548.47
	(2, 2, 2, ±2, 4)	1953.05
	(2, 2, 2, 0, 4)	−128.63
$\lambda_1 = 3$	(3, 0, 0, 0, 3)	−68.52
	(3, 0, 1, 0, 4)	839.36
	(3, 0, 2, 2, 5)	407.71
	(3, 0, 3, 0, 6)	−107.84
	(3, 2, 0, 0, 3)	137.84
	(3, 2, 1, 0, 4)	−1112.08
	(3, 2, 2, ±2, 5)	−540.28
	(3, 2, 3, ±2, 6)	−188.47
	(3, 2, 3, 0, 6)	142.53
$\lambda_1 = 4$	(4, 0, 1, 0, 5)	−232.47
	(4, 0, 2, 2, 6)	−147.79
	(4, 2, 1, 0, 5)	206.02
	(4, 2, 2, ±2, 6)	130.58
	(4, 4, 1, 0, 5)	175.29
	(4, 4, 2, ±2, 6)	108.51

[a]The normalization of expansion functions is given in Table 8 on page 22 of the user manual (see the Supporting Information).

2. Isotropic term $v_{00000}(R)$ has a minimum near R = 6.6 Bohr and a well depth of ∼10 000 cm^{-1}. Interestingly, the dipole−dipole interaction term $v_{10102}(R)$ is approximately 3 times larger. The next most important term is $v_{22103}(R)$ that corresponds to the quadrupole−dipole interaction, and the next $v_{22224}(R)$ corresponds to the quadrupole−quadrupole interaction. Their magnitudes are roughly 3 and 6 times smaller, respectively, than the dipole−dipole term but are still comparable to the isotropic interaction term. The next most significant is hexapole−dipole term $v_{32104}(R)$, followed by the group of $v_{30104}(R)$, $v_{32225}(R)$, $v_{30225}(R)$, and $v_{42105}(R)$ terms that include interactions up to the octupole. These are ∼1 order of magnitude smaller than the dipole−dipole term. All 23 dependencies $v_{\lambda_1\mu_1\lambda_2\mu_2\lambda}(R)$ are shown in Figure 2, and the 12 largest terms are labeled. The values of expansion coefficients near R = 8 Bohr are listed in Table 1. One can see that the magnitude of the largest term (dipole−dipole) is close to 14 251 cm^{-1}, while that for the smallest included term is only ∼68.5 cm^{-1}.

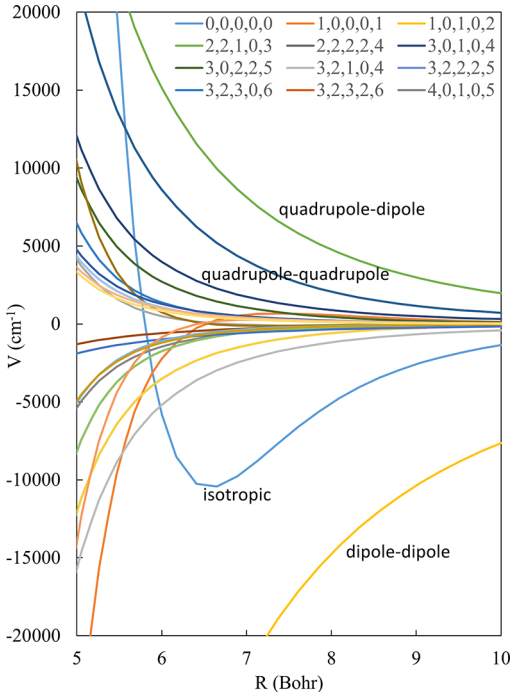

Figure 2. Radial dependence of 23 expansion coefficients $v_{\lambda_1\mu_1\lambda_2\mu_2\lambda}(R)$ for the H_2O + H_2O interaction potential. The four most important expansion terms are labeled, and the largest 12 are labeled by $\lambda_1\mu_1\lambda_2\mu_2\lambda$.

To quantify the accuracy of PES expansion, we computed by direct numerical integration the values of matrix elements for a small subset of states ($0_{00}0_{00}$, $0_{00}1_{11}$, $0_{00}2_{02}$, $1_{11}0_{00}$, $1_{11}1_{11}$, $1_{11}2_{02}$, $2_{02}0_{00}$, $2_{02}1_{11}$, and $2_{02}2_{02}$) at two molecule−molecule distances (near R = 6 and 8 Bohr). Direct integration is numerically expensive and is impractical for calculations of the entire matrix for the H_2O + H_2O system, but it can be employed to obtain a set of benchmark data for a smaller subset of transitions. In Figure 3, we plot a comparison of

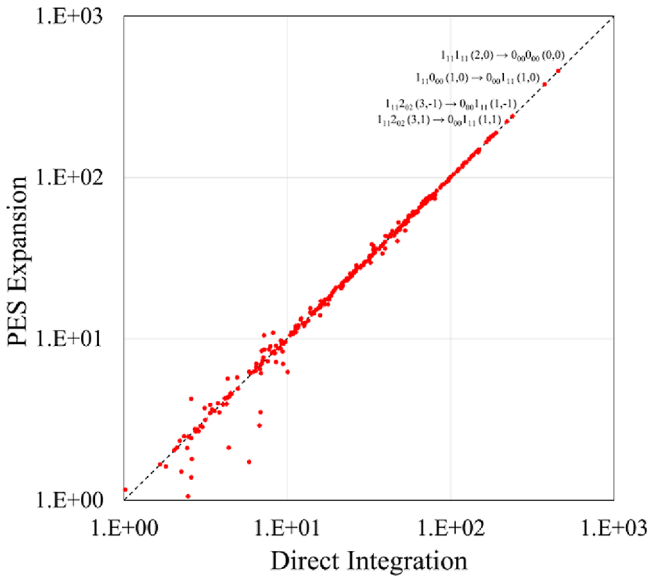

Figure 3. Comparison of matrix elements for the H_2O + H_2O system computed analytically (using PES expansion) vs those computed by direct numerical integration. State-to-state transitions that correspond to the four largest matrix elements are labeled. The numbers in parentheses correspond to the initial and final values of the overall (j, m).

matrix elements obtained by direct integration versus those computed analytically using PES expansion. We can see that the magnitudes of the larger matrix elements exceed 500 cm^{-1} and those are computed very accurately. Many matrix elements fall in the range between 10 and 200 cm^{-1}, and for those, the PES expansion also works reasonably well. However, smaller matrix elements (<10 cm^{-1}) indicate visible errors due to truncation of the PES expansion. One option is to recompute these elements with a larger PES expansion (which can be numerically challenging), and another option is to neglect

https://doi.org/10.1021/acs.jpclett.2c03328
J. Phys. Chem. Lett. 2023, 14, 817−824

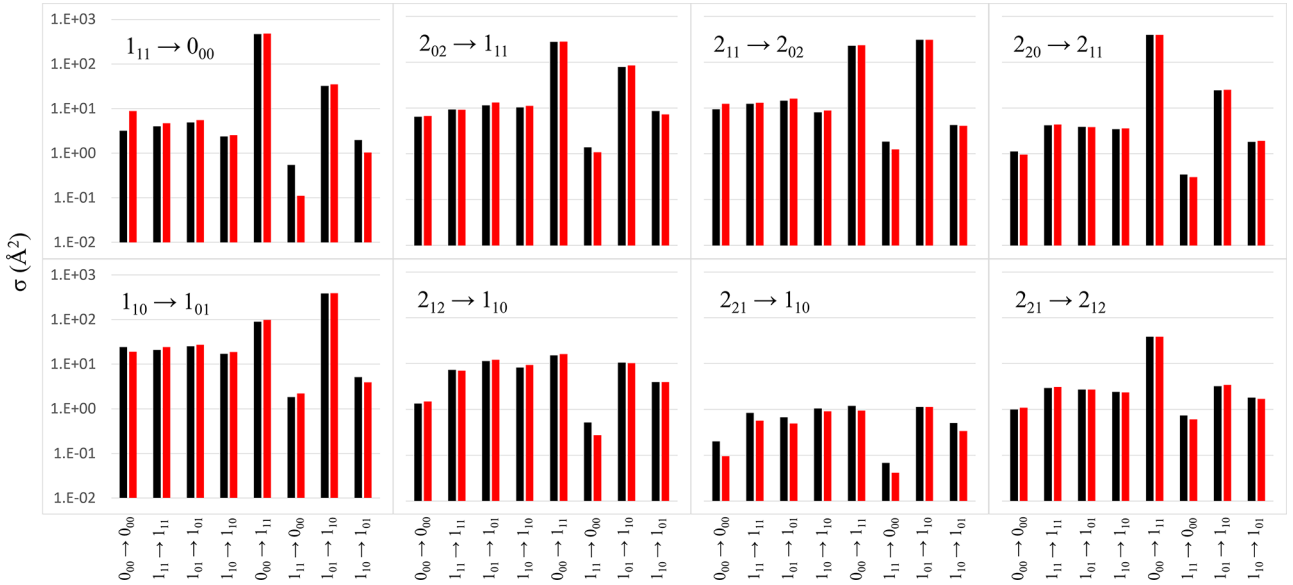

Figure 4. Comparison of state-to-state transition cross sections (in units of square angstroms) computed by the fully coupled CC-MQCT method (black bars) and the approximate AT-MQCT method (red bars). For the "target" molecule, four transitions for *para* water are presented in the top row and another four transitions for *ortho* water are presented in the bottom row. The horizontal axis lists various state-to-state transitions in the "quencher" molecule (64 transitions total).

them during the propagation of MQCT trajectories (on the basis of their relatively small values).

On the basis of the analysis presented above, the state-to-state transition matrix for the $H_2O + H_2O$ system was analyzed and truncated to retain only the matrix elements with magnitudes of >10 cm^{-1}. This resulted in 100 319 matrix elements (transitions) included in the propagation of the equations of motion (eqs 1−5) presented above. Expansion coefficients were computed on a grid of 171 points that was chosen to be denser in the short-range region (ΔR = 0.1 Bohr near R = 4 Bohr) and sparser in the long-range region of the PES (ΔR = 2.5 Bohr near R = 100 Bohr). Matrix elements for the individual state-to-state transitions were computed on the same R grid using the formulas of Table 9 of the user manual (see the Supporting Information). The MQCT code constructs cubic splines of these data to propagate trajectories. For the $H_2O + H_2O$ collision, we considered one value of the kinetic energy U = 533 cm^{-1}. The maximum value of the impact parameter was set at 60 Bohr, and the initial molecule−molecule distance was 100 Bohr. Values of orbital angular momentum up to $l_{max} \sim 550$ were required. To facilitate CC-MQCT calculations that become costly in this case, we used a step $\Delta l \sim 19$ [keyword DL = 19 (see page 26 of the user manual)]. This resulted in propagation of 29 MQCT trajectories for each combination of j and m of the initial state. Convergence of cross sections with respect to the value of Δl was within the range of 4−8% for different transitions. Calculations were carried out in parallel using 128 processors of HPC *Raj* at Marquette University (AMD Rome 2 GHz processors, 512 GB of memory). Sixteen processors were used to propagate each trajectory. To have a meaningful comparison, both CC-MQCT and AT-MQCT trajectories were propagated using the same standard RK4 propagator with a constant time step of 100 au.

Independent sets of calculations were carried out for *para*−*para*, *para*−*ortho*, *ortho*−*para*, and *ortho*−*ortho* combinations of the rotational states of two collision partners. The approximate AT-MQCT calculations were ∼3 times faster than the fully coupled CC-MQCT calculations (using the RK4 propagator with a constant time step of 100 au in both cases). In Figure 4, the results of the two methods are compared. The top row gives four examples of state-to-state transitions in *para* water, while the bottom row gives four examples of transitions in *ortho* water. The vertical axis gives the values of integral cross sections for state-to-state transitions in the "target" molecule (in units of square angstroms), while the horizontal axis lists several possible transitions in the "quencher" molecule (including both *para* and *ortho* water).

Overall, 64 state-to-state transitions of various symmetries are presented in Figure 4, focusing on transitions between various excited states of the quencher within the j = 2 manifold. For most of them, the results of the two MQCT methods are very similar. In particular, for all transitions with large cross sections (11 transitions in Figure 4), the results of approximate AT-MQCT are nearly identical to the results of fully coupled CC-MQCT. Visible differences are found for those transitions that exhibit small values of cross sections (only one transition in Figure 4). In some cases, AT-MQCT slightly overestimates the values of small cross sections, while in other cases, it slightly underestimates them. Because, overall, these processes are less important, we can conclude that the accuracy of AT-MQCT approximation is quite satisfactory. In the past, a similar good agreement between AT-MQCT and CC-MQCT was obtained for the $H_2O + H_2$ system.[27]

For the modeling of collisional energy transfer, it is often necessary to compute the so-called thermally averaged cross sections for state-to-state transitions in the "target" molecule, obtained by summation over the final states and averaging over the initial states of the "quencher" molecule (using the thermal distribution of quencher states at a given temperature), which includes both *para* and *ortho* states of the quencher combined with appropriate weights.[39] We computed such thermally averaged cross sections for several *para* and *ortho* states of the "target" molecule assuming a Boltzman distribution of "quencher" states at 800 K. To take full advantage of AT-

https://doi.org/10.1021/acs.jpclett.2c03328
J. Phys. Chem. Lett. 2023, 14, 817−824

MQCT, the adaptive step size procedure specific to this method was enabled using the keyword AT_ADAPTOL = 0.0005 (see page 12 of the user manual). This resulted in an acceleration of AT-MQCT calculations by a factor of 76 compared to CC-MQCT calculations. The results of the two calculations are presented in Figure 5. We see that the two sets

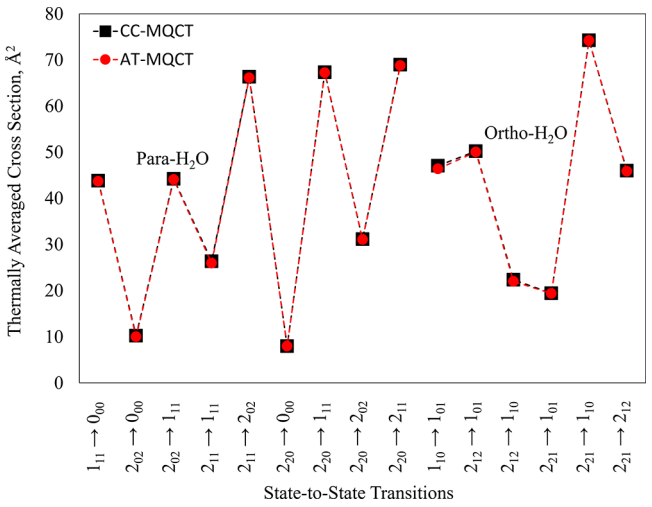

Figure 5. Comparison of thermally averaged cross sections computed by the fully coupled CC-MQCT method (black squares) and the approximate AT-MQCT method (red circles) for several state-to-state transitions in *para* and *ortho* water.

of data are barely distinguishable. The differences we saw in the individual state-to-state transitions in Figure 4 are largely washed out by thermal averaging in Figure 5, where the largest deviation is just slightly more than 1% of the cross section value. One conclusion is that AT-MQCT is particularly well suited for the calculations of thermally averaged cross sections. The second observation is that even in the thermally averaged cross sections the quantum propensity rules remain important. Namely, from Figure 5, one can notice that all transitions with odd values of Δk_a and Δk_c exhibit systematically larger cross sections, compared to transitions with even values of Δk_a and Δk_c that are always smaller, and this is valid for the *para* and *ortho* states of water.

In this paper, we present a new version of the MQCT program that includes an important addition, an adiabatic trajectory method or AT-MQCT, in which the propagations of the equations of motion for classical and quantum parts of the system are decoupled. This approximate method is much faster, which enables calculations for larger molecular systems and at higher collision energies than was possible before. Because the method is general, it can be applied to any molecule + molecule inelastic scattering problem. In MQCT_2022, an adiabatic trajectory approximation is implemented for all system types up to the most general case of an asymmetric-top rotor + asymmetric-top rotor system.

The results presented here for the H_2O + H_2O system, which is one example of an asymmetric-top + asymmetric-top system, indicate that AT-MQCT is rather accurate for prediction of state-to-state transition cross sections between the individual rotational states of two collision partners, and this is valid for all combinations of state symmetries (such as the *para* and *ortho* states of each collision partner). Moreover, thermally averaged cross sections obtained by AT-MQCT are nearly identical to those obtained by the fully coupled MQCT method (CC-MQCT). The calculations of a database of thermally averaged cross sections for H_2O + H_2O collisional energy transfer, very much in demand in the astrochemistry community, are ongoing, in which we use the rotational basis set of 1064 states of the water + water system that includes 28 states of the target molecule up to j_1 = 8 combined with 38 states of the quencher up to j_2 = 10, in each of the four independent calculations for the *ortho* and *para* combination. The results will be reported elsewhere.

A summary of MQCT_2022 code capabilities is presented herein, and a detailed user manual, including the list of all keywords for the expert-level calculations, is provided in the Supporting Information. In addition to AT-MQCT, the new version of the MQCT package includes many fixes (found in the previous version of the code) and several major improvements for efficiency and portability. See the user manual for further information. At present, the code is available from authors by reasonable request. In the near future, the code will be made available to the community through GitHub.

■ ASSOCIATED CONTENT

Supporting Information

The Supporting Information is available free of charge at https://pubs.acs.org/doi/10.1021/acs.jpclett.2c03328.

Complete and updated user manual for MQCT_2022, which includes a description of all system types available in the MQCT_2022 program, a list of all required and optional keywords, suggested strategies for the efficient use of the code, a procedure for connecting the external PES, and a summary of equations used to compute matrix elements (PDF)

■ AUTHOR INFORMATION

Corresponding Author

Dmitri Babikov − *Department of Chemistry, Marquette University, Milwaukee, Wisconsin 53201-1881, United States*; orcid.org/0000-0002-4667-7645; Email: dmitri.babikov@mu.edu

Authors

Bikramaditya Mandal − *Department of Chemistry, Marquette University, Milwaukee, Wisconsin 53201-1881, United States*; orcid.org/0000-0001-6682-0376

Carolin Joy − *Department of Chemistry, Marquette University, Milwaukee, Wisconsin 53201-1881, United States*

Dulat Bostan − *Department of Chemistry, Marquette University, Milwaukee, Wisconsin 53201-1881, United States*

Alexander Eng − *Department of Chemistry, Marquette University, Milwaukee, Wisconsin 53201-1881, United States*

Complete contact information is available at: https://pubs.acs.org/10.1021/acs.jpclett.2c03328

Notes

The authors declare no competing financial interest.

https://doi.org/10.1021/acs.jpclett.2c03328
J. Phys. Chem. Lett. 2023, 14, 817−824

■ ACKNOWLEDGMENTS

This research was partially supported by the NASA Astrophysics Program (Grant NNX17AH16G) and partially by the National Science Foundation (NSF) Chemistry Program (Grant CHE-2102465). D. Babikov acknowledges the support of a Way Klingler Research Fellowship. B.M. acknowledges the support of Denis J. O'Brien and Eisch Fellowships. A.E. was supported by the Graduate Summer Research Program at Marquette University. The authors used resources of the National Energy Research Scientific Computing Center, which is supported by the Office of Science of the U.S. Department of Energy under Contract DE-AC02-5CH11231. This research also used HPC resources at Marquette University funded in part by the NSF Grant CNS-1828649 (MRI: Acquisition of iMARC: High Performance Computing for STEM Research and Education in Southeast Wisconsin).

■ REFERENCES

(1) Wiesenfeld, L. Quantum Nature of Molecular Vibrational Quenching: Water–Molecular Hydrogen Collisions. *J. Chem. Phys.* **2021**, *155* (7), 071104.
(2) Kendrick, B. K.; Hazra, J.; Balakrishnan, N. Geometric Phase Appears in the Ultracold Hydrogen Exchange Reaction. *Phys. Rev. Lett.* **2015**, *115* (15), 153201.
(3) Bossion, D.; Scribano, Y.; Lique, F.; Parlant, G. Ro-Vibrational Excitation of H_2 by H Extended to High Temperatures. *Mon. Not. R. Astron. Soc.* **2018**, *480* (3), 3718−3724.
(4) Faure, A.; Wiesenfeld, L.; Wernli, M.; Valiron, P. The Role of Rotation in the Vibrational Relaxation of Water by Hydrogen Molecules. *J. Chem. Phys.* **2005**, *123* (10), 104309.
(5) van der Avoird, A.; Loreau, J.; Alexander, M. H.; van de Meerakker, S. Y. T.; Dagdigian, P. J. Resonances in Rotationally Inelastic Scattering of NH_3 and ND_3 with H_2. *J. Chem. Phys.* **2015**, *143* (4), 044312.
(6) Surin, L. A.; Tarabukin, I. V.; Schlemmer, S.; Breier, A. A.; Giesen, T. F.; McCarthy, M. C.; van der Avoird, A. Rotational Spectroscopy of the NH_3–H_2 Molecular Complex. *Astrophys. J.* **2017**, *838* (1), 27.
(7) Gao, Z.; Loreau, J.; Van Der Avoird, A.; Van De Meerakker, S. Y. T. Direct Observation of Product-Pair Correlations in Rotationally Inelastic Collisions of ND_3 with D_2. *Phys. Chem. Chem. Phys.* **2019**, *21* (26), 14033−14041.
(8) Paci, J. T.; Minton, T. K.; Schatz, G. C. Hyperthermal Oxidation of Graphite and Diamond. *Acc. Chem. Res.* **2012**, *45* (11), 1973−1981.
(9) Shpilman, Z.; Gouzman, I.; Grossman, E.; Shen, L.; Minton, T. K.; Paci, J. T.; Schatz, G. C.; Akhvlediani, R.; Hoffman, A. Oxidation and Etching of CVD Diamond by Thermal and Hyperthermal Atomic Oxygen. *J. Phys. Chem. C* **2010**, *114* (44), 18996−19003.
(10) Cho, J.; Tao, Y.; Georgievskii, Y.; Klippenstein, S. J.; Jasper, A. W.; Sivaramakrishnan, R. The Role of Collisional Energy Transfer in the Thermal and Prompt Dissociation of 1-Methyl Allyl. *Proc. Combust. Inst.* **2022**, DOI: 10.1016/j.proci.2022.07.155.
(11) Troya, D.; Schatz, G. C. Theoretical Studies of Hyperthermal O (3^P) Collisions with Hydrocarbon Self-Assembled Monolayers. *J. Chem. Phys.* **2004**, *120* (16), 7696−7707.
(12) Jasper, A. W. Predicting Third-Body Collision Efficiencies for Water and Other Polyatomic Baths. *Faraday Discuss.* **2022**, *238*, 68.
(13) Daniel, F.; Dubernet, M.-L.; Grosjean, A. Rotational Excitation of 45 Levels of Ortho/Para-H_2O by Excited Ortho/Para-H_2 from 5 to 1500 K: State-to-State, Effective, and Thermalized Rate Coefficients. *Astron. Astrophys.* **2011**, *536*, A76.
(14) Faure, A.; Wiesenfeld, L.; Scribano, Y.; Ceccarelli, C. Rotational Excitation of Mono-and Doubly-Deuterated Water by Hydrogen Molecules. *Mon. Not. R. Astron. Soc.* **2012**, *420* (1), 699−704.
(15) Denis-Alpizar, O.; Stoecklin, T.; Dutrey, A.; Guilloteau, S. Rotational Relaxation of HCO^+ and DCO^+ by Collision with H2. *Mon. Not. R. Astron. Soc.* **2020**, *497* (4), 4276−4281.
(16) Ben Khalifa, M.; Quintas-Sánchez, E.; Dawes, R.; Hammami, K.; Wiesenfeld, L. Rotational Quenching of an Interstellar Gas Thermometer: CH_3CN···He Collisions. *Phys. Chem. Chem. Phys.* **2020**, *22*, 17494.
(17) Faure, A.; Szalewicz, K.; Wiesenfeld, L. Potential Energy Surface and Rotational Cross Sections for Methyl Formate Colliding with Helium. *J. Chem. Phys.* **2011**, *135* (2), 024301.
(18) Faure, A.; Dagdigian, P. J.; Rist, C.; Dawes, R.; Quintas-Sánchez, E.; Lique, F.; Hochlaf, M. Interaction of Chiral Propylene Oxide (CH_3CHCH_2O) with Helium: Potential Energy Surface and Scattering Calculations. *ACS Earth Sp. Chem.* **2019**, *3* (6), 964−972.
(19) Beck, M. H.; Jäckle, A.; Worth, G. A.; Meyer, H.-D. The Multiconfiguration Time-Dependent Hartree (MCTDH) Method: A Highly Efficient Algorithm for Propagating Wavepackets. *Phys. Rep.* **2000**, *324* (1), 1−105.
(20) Meyer, H.-D.; Manthe, U.; Cederbaum, L. S. The Multi-Configurational Time-Dependent Hartree Approach. *Chem. Phys. Lett.* **1990**, *165* (1), 73−78.
(21) Ndengué, S.; Scribano, Y.; Gatti, F.; Dawes, R. State-to-State Inelastic Rotational Cross Sections in Five-Atom Systems with the Multiconfiguration Time Dependent Hartree Method. *J. Chem. Phys.* **2019**, *151* (13), 134301.
(22) Ndengué, S.; Dawes, R.; Gatti, F.; Meyer, H.-D. Atom-Triatom Rigid Rotor Inelastic Scattering with the MultiConfiguration Time Dependent Hartree Approach. *Chem. Phys. Lett.* **2017**, *668*, 42−46.
(23) Konings, M.; Desrousseaux, B.; Lique, F.; Loreau, J. Benchmarking an Improved Statistical Adiabatic Channel Model for Competing Inelastic and Reactive Processes. *J. Chem. Phys.* **2021**, *155* (10), 104302.
(24) Loreau, J.; Faure, A.; Lique, F. Scattering of CO with H_2O: Statistical and Classical Alternatives to Close-Coupling Calculations. *J. Chem. Phys.* **2018**, *148* (24), 244308.
(25) Semenov, A.; Babikov, D. Mixed Quantum/Classical Approach for Description of Molecular Collisions in Astrophysical Environments. *J. Phys. Chem. Lett.* **2015**, *6* (10), 1854−1858.
(26) Babikov, D.; Semenov, A. Recent Advances in Development and Applications of the Mixed Quantum/Classical Theory for Inelastic Scattering. *J. Phys. Chem. A* **2016**, *120* (3), 319−331.
(27) Mandal, B.; Semenov, A.; Babikov, D. Adiabatic Trajectory Approximation within the Framework of Mixed Quantum/Classical Theory. *J. Phys. Chem. A* **2020**, *124* (47), 9877−9888.
(28) Semenov, A.; Babikov, D. Mixed Quantum/Classical Theory of Rotationally and Vibrationally Inelastic Scattering in Space-Fixed and Body-Fixed Reference Frames. *J. Chem. Phys.* **2013**, *139* (17), 174108.
(29) Semenov, A.; Babikov, D. Mixed Quantum/Classical Calculations of Total and Differential Elastic and Rotationally Inelastic Scattering Cross Sections for Light and Heavy Reduced Masses in a Broad Range of Collision Energies. *J. Chem. Phys.* **2014**, *140* (4), 044306.
(30) Semenov, A.; Babikov, D. Accurate Calculations of Rotationally Inelastic Scattering Cross Sections Using Mixed Quantum/Classical Theory. *J. Phys. Chem. Lett.* **2014**, *5* (2), 275−278.
(31) Mandal, B.; Semenov, A.; Babikov, D. Calculations of Differential Cross Sections Using Mixed Quantum/Classical Theory of Inelastic Scattering. *J. Phys. Chem. A* **2018**, *122* (30), 6157−6165.
(32) Semenov, A.; Babikov, D. Inelastic Scattering of Identical Molecules within Framework of the Mixed Quantum/Classical Theory: Application to Rotational Excitations in H_2 + H_2. *J. Phys. Chem. A* **2016**, *120* (22), 3861−3866.
(33) Semenov, A.; Babikov, D. Mixed Quantum/Classical Theory for Molecule-Molecule Inelastic Scattering: Derivations of Equations and Application to N_2 + H_2 System. *J. Phys. Chem. A* **2015**, *119* (50), 12329−12338.
(34) Semenov, A.; Dubernet, M.-L. L.; Babikov, D. Mixed Quantum/Classical Theory for Inelastic Scattering of Asymmetric-Top-Rotor + Atom in the Body-Fixed Reference Frame and

Application to the H_2O + He System. *J. Chem. Phys.* **2014**, *141* (11), 114304.
(35) Mandal, B.Development of MQCT Method for Calculations of Collisional Energy Transfer for Astrochemistry and Planetary Atmospheres. Ph.D. Thesis, Marquette University, Milwaukee, WI, 2021.
(36) Hong, Q.; Sun, Q.; Bartolomei, M.; Pirani, F.; Coletti, C. Inelastic Rate Coefficients Based on an Improved Potential Energy Surface for N_2+ N_2 Collisions in a Wide Temperature Range. *Phys. Chem. Chem. Phys.* **2020**, *22* (17), 9375−9387.
(37) Besemer, M.; Tang, G.; Gao, Z.; van der Avoird, A.; Groenenboom, G. C.; van de Meerakker, S. Y. T.; Karman, T. Glory Scattering in Deeply Inelastic Molecular Collisions. *Nat. Chem.* **2022**, *14*, 664.
(38) Semenov, A.; Mandal, B.; Babikov, D. MQCT: User-Ready Program for Calculations of Inelastic Scattering of Two Molecules. *Comput. Phys. Commun.* **2020**, *252*, 107155.
(39) Boursier, C.; Mandal, B.; Babikov, D.; Dubernet, M. L. New H_2O−H_2O Collisional Rate Coefficients for Cometary Applications. *Mon. Not. R. Astron. Soc.* **2020**, *498* (4), 5489−5497.
(40) Semenov, A.; Babikov, D. A. MQCT. I. Inelastic Scattering of Two Asymmetric-Top Rotors with Application to H_2O+ H_2O. *J. Phys. Chem. A* **2017**, *121* (26), 4855−4867.
(41) Mandal, B.; Joy, C.; Semenov, A.; Babikov, D. Mixed Quantum/Classical Theory for Collisional Quenching of PAHs in the Interstellar Media. *ACS Earth Sp. Chem.* **2022**, *6* (3), 521−529.
(42) Semenov, A.; Babikov, D. Equivalence of the Ehrenfest Theorem and the Fluid-Rotor Model for Mixed Quantum/Classical Theory of Collisional Energy Transfer. *J. Chem. Phys.* **2013**, *138* (16), 164110.
(43) Semenov, A.; Ivanov, M.; Babikov, D. Ro-Vibrational Quenching of CO (v = 1) by He Impact in a Broad Range of Temperatures: A Benchmark Study Using Mixed Quantum/Classical Inelastic Scattering Theory. *J. Chem. Phys.* **2013**, *139* (7), 074306.
(44) Bockelée-Morvan, D.; Calmonte, U.; Charnley, S.; Duprat, J.; Engrand, C.; Gicquel, A.; Hässig, M.; Jehin, E.; Kawakita, H.; Marty, B.; et al. Cometary Isotopic Measurements. *Space Sci. Rev.* **2015**, *197* (1), 47−83.
(45) Wirström, E. S.; Bjerkeli, P.; Rezac, L.; Brinch, C.; Hartogh, P. Effect of the 3D Distribution on Water Observations Made with the SWI-I. Ganymede. *Astron. Astrophys.* **2020**, *637*, A90.
(46) Hutson, J. M.; Green, S.*MOLSCAT Computer Code*, ver. 14; Collaborative Computational Project, 1994; No. 6.
(47) Hutson, J. M.; Le Sueur, C. R.*MOLSCAT, BOUND, and FIELD*, ver. 2020.0; 2020.
(48) Jankowski, P.; Murdachaew, G.; Bukowski, R.; Akin-Ojo, O.; Leforestier, C.; Szalewicz, K. Ab Initio Water Pair Potential with Flexible Monomers. *J. Phys. Chem. A* **2015**, *119* (12), 2940−2964.
(49) Cencek, W.; Szalewicz, K.; Leforestier, C.; van Harrevelt, R.; van der Avoird, A. An Accurate Analytic Representation of the Water Pair Potential. *Phys. Chem. Chem. Phys.* **2008**, *10* (32), 4716−4731.

https://doi.org/10.1021/acs.jpclett.2c03328
J. Phys. Chem. Lett. 2023, 14, 817−824